nature neuroscience

Nicotinic control of axon excitability regulates thalamocortical transmission

Hideki Kawai, Ronit Lazar & Raju Metherate

The thalamocortical pathway, a bundle of myelinated axons that arises from thalamic relay neurons, carries sensory information to the neocortex. Because axon excitation is an obligatory step in the relay of information from the thalamus to the cortex, it represents a potential point of control. We now show that, in adult mice, the activation of nicotinic acetylcholine receptors (nAChRs) in the initial portion of the auditory thalamocortical pathway modulates thalamocortical transmission of information by regulating axon excitability. Exogenous nicotine enhanced the probability and synchrony of evoked action potential discharges along thalamocortical axons *in vitro*, but had little effect on synaptic release mechanisms. *In vivo*, the blockade of nAChRs in the thalamocortical pathway reduced sound-evoked cortical responses, especially those evoked by sounds near the acoustic threshold. These data indicate that endogenous acetylcholine activates nAChRs in the thalamocortical pathway to lower the threshold for thalamocortical transmission and to increase the magnitude of sensory-evoked cortical responses. Our results show that a neurotransmitter can modulate sensory processing by regulating conduction along myelinated thalamocortical axons.

Thalamic neurons transmit sensory information that is crucial for cortical function; for example, they establish topographic maps in sensory cortex[1]. The transmission of information from thalamus to cortex seems to be highly effective, with axon myelination to ensure faithful transmission and highly reliable neurotransmitter release at thalamocortical synapses[2–4], but depends on several processes that are subject to neuromodulatory regulation[5–8], including synaptic integration in the somata of thalamic neurons and synaptic release at thalamocortical terminals. The intervening processes—namely, action potential initiation and propagation along thalamocortical axons—could also influence thalamocortical efficacy by, for example, establishing the threshold for thalamocortical transmission and synchronizing action potentials to drive cortical neurons to threshold[9,10]. A full understanding of thalamocortical relay mechanisms calls for detailed knowledge of each of these processes, including potential points of regulation.

The neurotransmitter acetylcholine (ACh) can influence thalamocortical processing via nAChRs in at least two ways. First, postsynaptic nAChRs can mediate depolarization in some thalamic[11,12] and cortical[13–15] neurons, potentially altering the integration of afferent inputs. Second, presynaptic nAChRs are thought to regulate neurotransmitter release, including release from thalamocortical terminals, in ways that can be independent of action potentials (tetrodotoxin-insensitive) or dependent on action potentials (tetrodotoxin-sensitive; also called 'preterminal' nAChRs)[16,17]. Recently, a potential third mechanism has been implicated: positron emission tomography (PET) studies using a radioactive nicotinic ligand in humans have shown that nAChRs are present in the white matter (myelinated axons) of sensory thalamocortical pathways[18]. It has been suggested that such receptors are being transported to the cortex, or might serve an unknown function in the white matter. To date, there has been no evidence that ACh—or any other neurotransmitter—acts on myelinated thalamocortical axons, even though neuromodulation of action potential initiation or propagation could powerfully regulate thalamocortical transmission. Here we use *in vitro* and *in vivo* preparations of the auditory thalamocortical pathway from the adult mouse to determine whether nAChRs regulate thalamocortical transmission. We show that activation of nAChRs in the initial portion of the pathway modulates thalamocortical transmission by regulating axon excitability.

RESULTS

Reliable thalamocortical synaptic transmission

Myelinated axons of auditory thalamic relay neurons course through the superior thalamic radiation (STR) before exiting the thalamus, where they join the internal capsule in the subcortical white matter, and eventually terminate in layers 3–4 of primary auditory cortex. We prepared auditory thalamocortical slices[19] from 2–3-month-old mice, and used 'minimal' stimulation to isolate monosynaptic thalamocortical responses in layer 3–4 neurons under voltage clamp. Neurons analyzed here showed adapting spike discharges with or without after-depolarization (that is, we excluded non-adapting, 'fast spiking' neurons). Stimulation of axons in the STR with intensity that increased in small increments resulted in a gradual increase in success probability for evoked excitatory postsynaptic currents (EPSCs) with little change in response amplitude (that is, 'minimal' or 'single axon' stimulation; **Fig. 1a**). The success rate reached a plateau near 100% (**Fig. 1b**), indicating that thalamocortical synaptic transmission is highly reliable[2,3,20].

Department of Neurobiology and Behavior and Center for Hearing Research, University of California, Irvine, 2205 McGaugh Hall, Irvine, California 92697-4550, USA. Correspondence should be addressed to R.M. (rmethera@uci.edu).

Received 7 June; accepted 9 July; published online 19 August 2007; doi:10.1038/nn1956

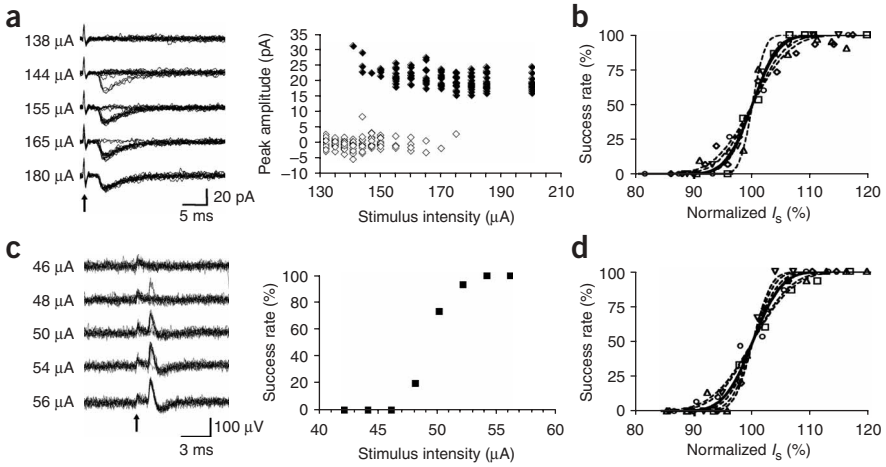

Figure 1 Postsynaptic and axon spike responses to stimulation of adult thalamocortical axons. (**a**) EPSCs evoked by minimal stimulation, recorded in layers 3–4 of auditory cortex. Left, sample traces (15 overlaid traces per stimulus intensity). Arrow indicates stimulus artifacts. Right, for the same neuron, peak amplitudes of response success (♦) and failure (◇) at each stimulus intensity. (**b**) Success rate for minimal EPSCs increased as a function of stimulus intensity. Data points for each experiment (symbols and dotted lines) were fitted with the threshold error function (see Methods) and averaged by normalizing I_s. Average relative spread was 5.06 ± 0.84 ($n = 5$) and was used to draw average function (solid line). (**c**) Axon spikes recorded extracellularly in cortical white matter. Left, sample traces (10 per stimulus intensity; arrow indicates stimulus). Right, success rates for the same axon, based on responses to >15 stimuli per intensity. (**d**) Success rates for axon spikes increased as a function of stimulus intensity. Curve fitting as in (**b**); relative spread averaged 5.48 ± 0.89 ($n = 5$), not different from that in (**b**) (ANOVA, $P = 0.90$).

Because the sigmoidal function of intensity against success rate (**Fig. 1b**) peaks near 100% (that is, there are no failures), the rising phase of the function reflects the efficacy of action potential initiation at the stimulus site. In particular, failures do not reflect branch point failure in the cortex or failure to release transmitter, as neither would be overcome by increasing stimulus intensity in the STR. To confirm this inference, we recorded action potentials (axon spikes) extracellularly from visually identified axons in the subcortical white matter while stimulating in the STR (**Fig. 1c**). The intensity-success rate functions for axon spikes (**Fig. 1d**) were similar to those for minimal EPSCs (**Fig. 1b**). Thus, the success rate of minimal responses depends on the probability of action potential induction in the STR, probably at the node of Ranvier nearest the stimulus site.

Nicotine raises probability of action potential induction

We then tested the effect of nicotine on thalamocortical EPSCs evoked by minimal stimulation. At stimulus intensities where success rates were sub-maximal, bath application of nicotine (<1 μM; see Methods for drug concentrations) increased success rate without altering response amplitude (**Fig. 2a–c**). Nicotine also did not affect the ratio of EPSC amplitudes elicited by paired-pulse stimulation (**Supplementary Fig. 1** online). The enhancement of success rate was mediated by nAChRs, as it was blocked by the antagonist dihydro-β-erythroidine (DHβE, 1 μM; **Fig. 2d**). In contrast to the results at sub-maximal stimulus intensities, at higher intensities that elicited ~100% success, nicotine had no effect on success rate (99.2 ± 0.8%, 97.9 ± 2.2% and

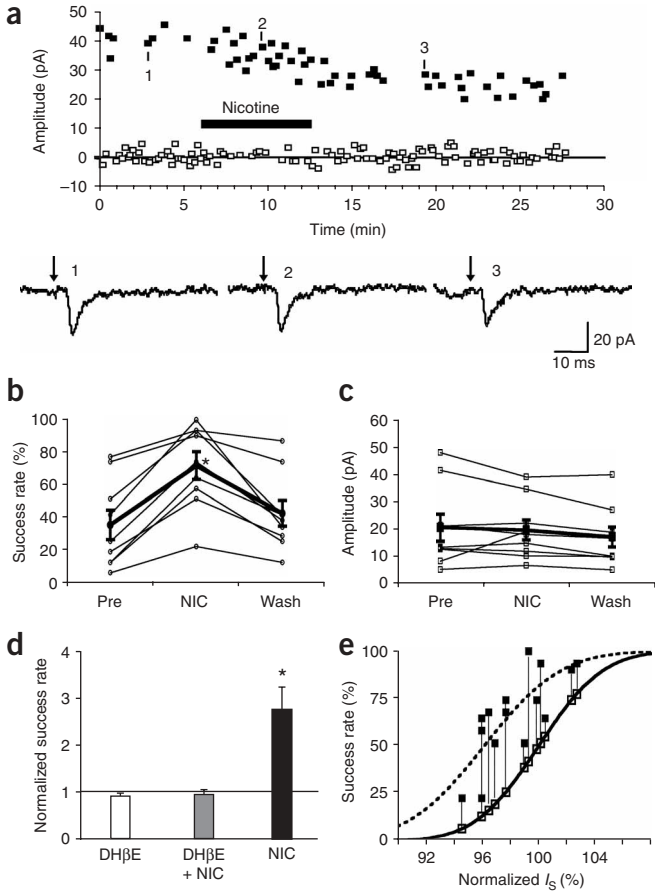

Figure 2 Nicotine enhances success rate for thalamocortical EPSCs. (**a**) In one example, successful responses (■) increased and failures (□) decreased during nicotine exposure (<1 μM). Numbers 1–3 refer to sample traces shown below. Arrows indicate stimulus onset. (**b**) Success rates before (Pre), during (NIC) and after (Wash) nicotine perfusion (5-min bin) for each experiment (thin lines) and on average (thick line, mean ± s.e.m., ANOVA, $^*P < 0.05$, $n = 9$). (**c**) Peak amplitudes did not change during nicotine treatment (ANOVA, $P = 0.89$). (**d**) The nicotinic antagonist DHβE (~1 μM) blocked the effect of nicotine on success rate. Success rates for DHβE alone (white bar, $n = 4$), nicotine with DHβE (gray bar, $n = 4$; DHβE was perfused ~6 min before nicotine), and nicotine alone (black bar, $n = 9$; data from (**b**) above) were normalized to baseline control. Error bars represent s.e.m. (ANOVA, $^*P < 0.05$). (**e**) Nicotine lowers stimulus intensities for threshold error function (threshold for action potential induction). Minimal response success rates for **b** and **Figure 4b** were combined (total of 15 cells). Success rates from before nicotine treatment (Pre; open squares) were aligned on the average error function (solid curve, see **Fig. 1b**). Success rates from during nicotine treatment (NIC; filled squares) were plotted directly above the corresponding control data (connected with vertical lines for each cell) and fitted with the threshold error function equation (dashed line, see Methods). *SI50* and *RS* values for NIC were 96.1% and 6.08 (with 95% confidence intervals between 2.25 and 9.92).

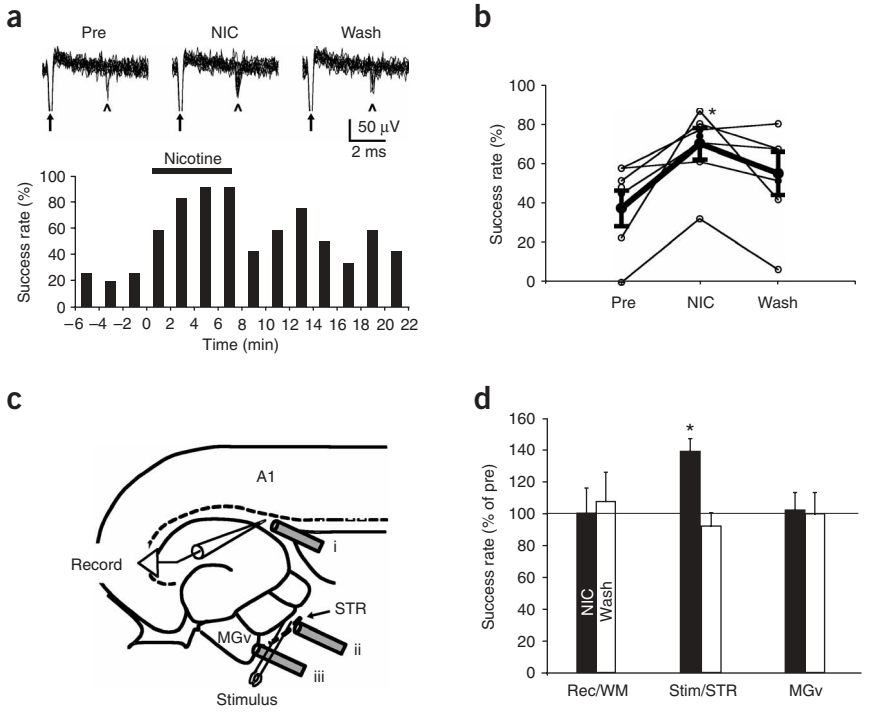

Figure 3 Nicotine enhances success rate for axon spikes in subcortical white matter. (**a**) Bath perfusion of nicotine increased axon spike success rate. Top, sample traces of axon spikes (arrowheads) before, during and after nicotine bath perfusion. Ten traces for each condition are overlaid. Arrows indicate stimulus artifacts. Bottom, for the same cell, time course of nicotine effect on success rate (2-min bins; horizontal bar represents duration of nicotine perfusion). (**b**) Axon spike success rate for each experiment (thin lines, each data point represents 5-min bin) and on average (thick line; ± s.e.m., $n = 6$, ANOVA, $^*P < 0.01$). Note in one experiment (the bottom thin line), that nicotine induced responses to a previously subthreshold stimulus. (**c**) A schematic diagram of a local perfusion experiment. Axon spikes initiated in the STR (stimulus) were recorded in the subcortical white matter (record). The perfusion needle was placed sequentially at three different locations: (i) the recording site in sub-cortical white matter; (ii) the stimulus site in the STR; and (iii) the MGv. (**d**) Local perfusion of nicotine (1 µM in the perfusion needle) increased success rates (5-min bin; ± s.e.m., ANOVA, $^*P < 0.05$) when applied to stimulus site in the STR (Stim/STR, $n = 9$), but not to recording site in white matter (Rec/WM, $n = 7$) or to the MGv ($n = 8$). Black bars are during nicotine, white bars are during wash.

98.9 ± 1.1% before, during and after nicotine; $n = 4$) or peak amplitude (21.8 ± 4.7 pA, 19.4 ± 4.1 pA, and 17.1 ± 4.3 pA before, during and after nicotine) and still did not affect paired-pulse ratio (**Supplementary Fig. 1**). Moreover, when tested in the absence of stimulus-evoked EPSCs, nicotine did not induce postsynaptic currents or alter the frequency or amplitude of spontaneous postsynaptic currents (**Supplementary Fig. 2** online) as would be expected if preterminal nAChRs, whose activation evokes action potentials, were involved[17,21]. Taken together, these data show that nicotinic enhancement of success rate does not involve presynaptic, preterminal or postsynaptic nAChRs. Rather, these data indicate that nAChRs regulate the probability of action potential induction in axons that pass the site of stimulation in the STR.

In **Fig. 2e**, we express the effect of nicotine as a change in the threshold function for action potential induction (see Methods for details). Nicotine shifted the function to lower stimulus intensities, indicating that it enhanced the excitability of thalamocortical axons.

Thalamic white matter is the site of nicotinic regulation

To test the idea that nAChRs regulate the excitability of myelinated thalamocortical axons, we performed several additional experiments. First, we found that bath perfusion of nicotine increased the success rate of axon spikes recorded from the sub-cortical white matter and evoked by STR stimulation (**Fig. 3a**,**b**). Then, we perfused nicotine locally, placing the tip of a perfusion needle at three sites: the recording site for axon spikes in subcortical white matter (1–2 mm 'downstream' of the stimulus site), the stimulus site in the STR, and the ventral division of the medial geniculate nucleus (MGv, ~0.5–1 mm upstream of the stimulus site), whose neurons are the source of thalamocortical axons passing through the STR (**Fig. 3c**). Control tests showed that local perfusion at the subcortical white matter or MGv does not affect the stimulus site in the STR (**Supplementary Fig. 3** and **Supplementary Methods** online). A consistent increase in success rate occurred only with nicotine perfusion at the stimulus site (**Fig. 3d**). Finally, we completely separated MGv from the thalamocortical pathway by cutting the STR upstream of the stimulus site at the MGv 'exit zone', and tested the effect of bath-applied nicotine on minimal EPSCs recorded in the cortex (**Fig. 4**). Nicotine still increased the success rate, with no change in peak amplitude. These data confirm that the locus of nicotinic action is at the stimulus site, that is, along myelinated thalamocortical axons.

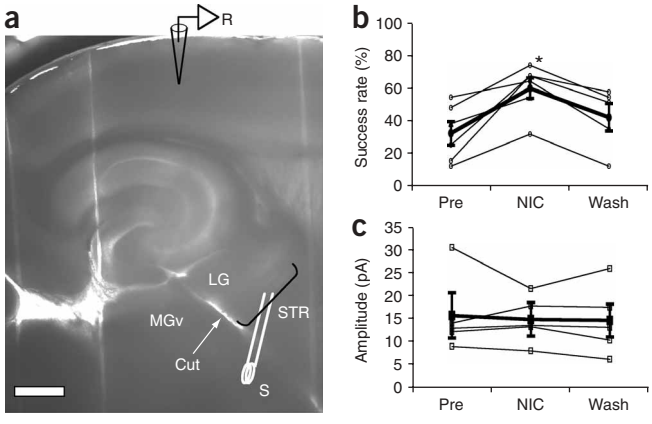

Figure 4 Minimal EPSCs in thalamocortical slices with MGv severed. (**a**) Thalamocortical slice with a cut (arrow) through the STR between MGv and the stimulus site (S). The STR is the bracketed region between the cut and the internal capsule, antero-medial to the lateral geniculate nucleus (LG). A typical recording site (R) in auditory cortex is also shown. Scale bar, 500 µm. (**b**) Nicotine increased the success rate (mean ± s.e.m., $n = 6$, ANOVA, $^*P < 0.05$; 5-min bin for each group). (**c**) Nicotine did not alter peak amplitude (mean ± s.e.m., ANOVA, $P = 0.84$).

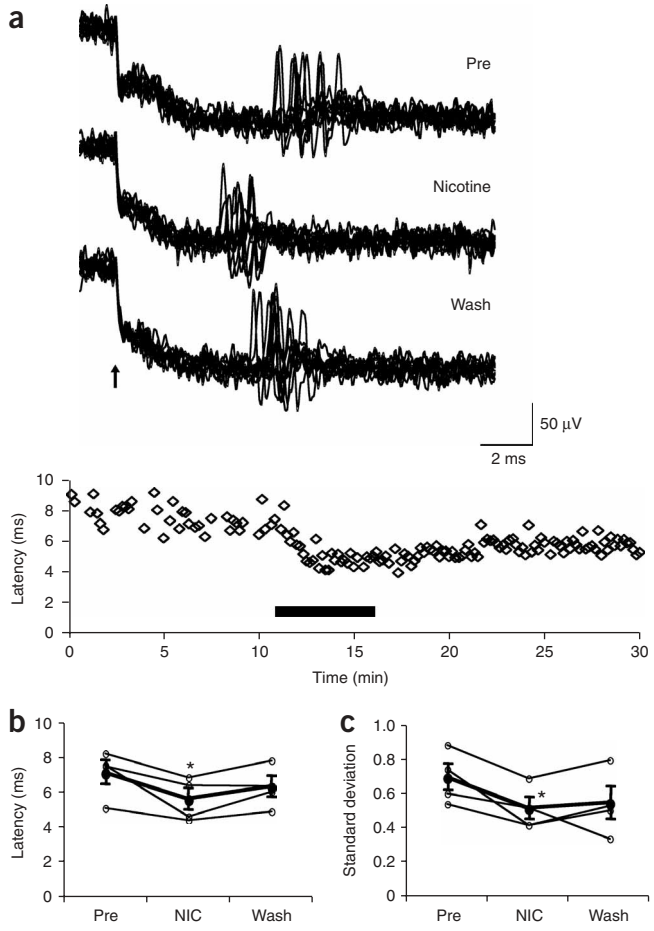

Figure 5 Nicotine decreases the latency and latency variability of axon spikes. (**a**) Top, sample traces of axon spikes elicited with low intensity/long duration stimulation (52 μA, 15 ms) before (Pre), during and after (Wash) nicotine (<1 μM). Ten traces for each group are shown; arrow indicates stimulus onset. Bottom, for the same cell, time course of effect on spike latency for successful responses. Horizontal bar shows approximate period of nicotine bath perfusion. (**b**,**c**) Axon spike latency and s.d. before, during and >5 min after nicotine perfusion for each experiment (thin lines, average of 10 pulses) and on average (thick line; ± s.e.m., $n = 4$, paired *t*-test, $^*P < 0.05$).

Nicotinic control of action potential timing

What might be the function of white matter nAChRs in thalamocortical transmission? First, nicotinic activation lowers the threshold for action potential induction (**Fig. 2e**) to stimulus intensities that normally do not induce action potentials. In experiments in which no or few successful responses were elicited (lowest success rates in **Figs. 2b and 3b**), nicotine enabled stimulus-induced action potentials, indicating that nicotinic activation works as a permissive gate for triggering action potentials when membrane potentials are near threshold.

Second, nicotinic activation could potentially decrease action potential latency because of a decrease in the time to reach threshold at the site of action potential induction. Indeed, analysis of onset latency for minimal EPSCs recorded in auditory cortex and axon spikes recorded in subcortical white matter showed small but significant decreases during nicotine treatment (**Supplementary Fig. 4** online; minimal EPSC latency reduced by 6 ± 2% below control, $n = 8$; axon spike latency reduced by 1.7 ± 0.3% below control, $n = 5$; mean ± s.e.m., ANOVA, $P < 0.005$ for both). However, it seemed that the relatively small change in onset latency during nicotine could be due to latencies being already near minimum owing to the intense, short-duration (0.2 ms) electrical stimulus. Conversely, the use of weaker but more prolonged stimuli would produce longer latencies and better mimic synaptic depolarization produced at dendrites and the soma, several hundred micrometers away[22,23]. To simulate such synaptic inputs, we placed a stimulus electrode in the MGv exit zone upstream of the STR ('Cut' area in **Fig. 4a**). After identification of axon spikes in subcortical white matter with short-duration stimulation, we lowered the stimulus intensity and prolonged the stimulus duration to 10–15 ms. Axon spike latency was delayed by 4.6 ± 0.5 ms ($n = 4$) compared with high intensity/short duration stimulation (at high intensity, onset latency = 2.5 ± 0.4 ms, s.d. 0.022 ± 0.005 ms). Under the weaker stimulus condition, nicotine decreased the onset latency to much greater extent (1.5 ± 0.5 ms, or 21 ± 6% decrease; $n = 4$, ANOVA, $P < 0.05$; **Fig. 5**), while increasing the success rate as expected (from 48.4 ± 5.9% to 76.6 ± 9.4%, ANOVA, $P < 0.05$). These data support the idea that nicotinic activation shortens the time taken to reach threshold.

Third, nicotinic activation might improve the synchronous timing of action potential discharge. The decrease in onset latency for axon spikes elicited with low intensity/long duration stimulation was associated with a decrease in latency variability (s.d.) to 25 ± 6% below control (ANOVA, $P < 0.05$; **Fig. 5c**). A similar decrease in onset variability was observed with high intensity/short duration stimulation for axon spikes (s.d. decreased to 28 ± 8% below control, $n = 5$, ANOVA, $P < 0.005$), but not minimal EPSCs (s.d. decreased to 5 ± 13% below control, $P > 0.05$; see **Supplementary Fig. 4**).

We found similar effects of nicotine on spike timing when we used monopolar stimulation to better confine the stimulus to a single site in the thalamocortical pathway. We recorded from single axons in subcortical white matter as described above, but axon spikes were elicited by cathodal (negative) current through a single electrode placed in the STR ~0.2–0.3 mm downstream of the MGv exit zone. Monopolar stimulation greatly limited the effective distance for eliciting axon spikes. Thus, when stimuli reliably elicited axon spikes, moving the stimulus electrode in ~50 μm steps perpendicular to the thalamocortical pathway resulted in a loss of effective stimulation within ~100 μm, indicating that there was a steep gradient of current density away from the electrode. With monopolar (as with bipolar) stimulation, lowering the stimulus intensity and prolonging its duration delayed the onset latency of axon spikes. As before, nicotine decreased spike latency and latency variability (latency decrease 5.5 ± 0.9%, ANOVA, $P < 0.001$; control latency 3.69 ± 0.19 ms, success rate 91.6 ± 5.2%; s.d. decrease 17.3 ± 2.1%, ANOVA, $P < 0.0001$, control s.d. 0.31 ± 0.07 ms; $n = 5$). Thus, the data obtained using monopolar stimulation are consistent with those obtained using bipolar stimulation, including data from slices cut between MGv and the STR (**Fig. 4**), and support the idea that the action of nicotine along the initial part of the thalamocortical pathway enhances thalamocortical transmission.

Overall, these *in vitro* data indicate that nicotinic activation in the initial portion of thalamocortical axons away from the somata of neurons in the MGv enhances axon excitability, reduces the latency of spiking, and promotes synchronous timing of action potential discharge.

Nicotinic control of thalamocortical transmission *in vivo*

We then investigated the functional importance of nicotinic regulation of axon excitability in the intact animal, by determining whether pharmacological blockade of nAChRs in the STR could affect sound-evoked responses in the auditory cortex of anesthetized mice. We used a

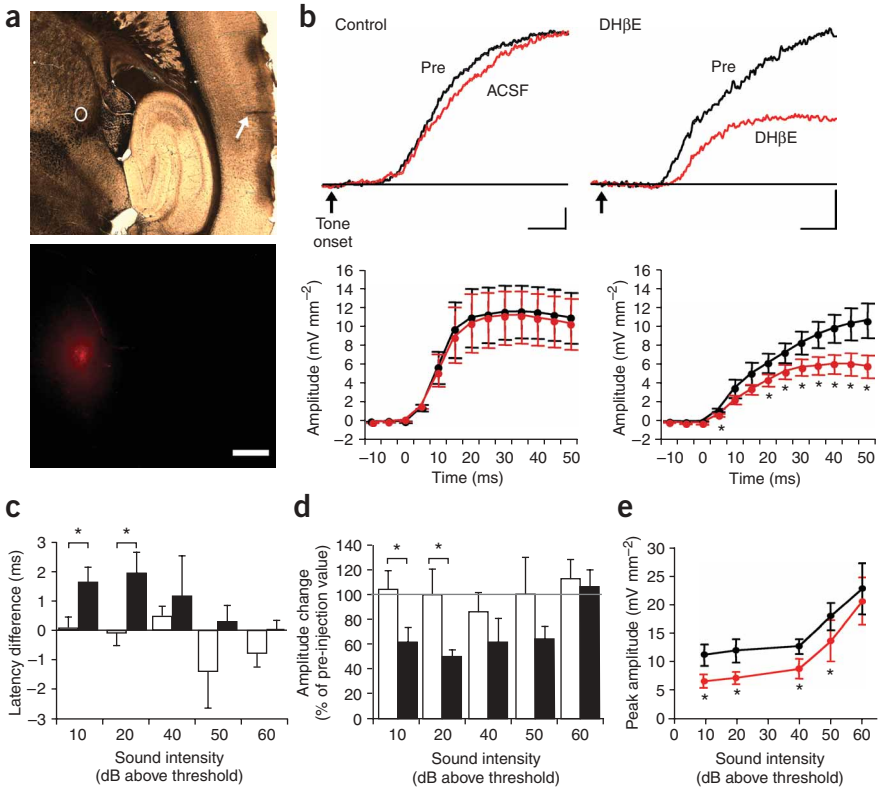

Figure 6 Blockade of nAChRs in thalamic white matter *in vivo* delays onset latency and decreases amplitude of tone-evoked responses in auditory cortex. (**a**) Sample images of a drug injection site. Top, a light microscope image of a brain section cut in the 'thalamocortical' plane. Bottom, the injection site (white circle in top image) was identified as the site of highest fluorescence intensity (same section as top). A multiprobe track is visible in the cortex (white arrow in top image). Scale bar, 500 μm. (**b**) Sample traces (top) and group average amplitudes (bottom) for CSD of early onset sink in auditory cortex before (black) and after (red) ACSF (left) and DHβE (right) injection in the STR. Stimulus is 10-dB characteristic frequency tone. Numbers on the abscissa indicate the end of a 5-ms period (see Methods). $n = 7$ for both ACSF and DHβE ($^*P < 0.05$, paired *t*-test). Scale: vertical bars are 3 mV mm^{-2}, and horizontal bars are 10 ms. (**c**,**d**) Change in onset latency (**c**) and initial (5-ms) amplitude (**d**) of early onset sink for different stimulus intensities (characteristic frequency tone). At 10 and 20 dB above acoustic threshold, onset latency increases and initial amplitude decreases after DHβE injection (filled bars) in comparison to ACSF injection (open bars) ($n = 7$, ANOVA, $^*P < 0.05$). (**e**) Peak amplitude of CSD main current sink before (black) and after (red) DHβE injection ($n = 7$ for 10, 20 and 60 dB; $n = 5$ for 40 and 50 dB; paired *t*-test, $^*P < 0.05$).

16-channel multiprobe electrode to record, simultaneously across all cortical layers, local field potentials (LFPs) evoked in response to pure tone stimuli at the characteristic frequency (the frequency of a sound at which the threshold of evoked response is lowest). Current source density (CSD) analysis, which reveals the putative sites of synaptic input (current sinks), identified one or two large current sinks in the middle to upper layers (~200–400 μm from the pia) generated by acoustic input. The earliest onset current sink in the input layers, which probably represents thalamocortical inputs, was either the main (largest amplitude) current sink, or an adjacent sink immediately below (the 'lower sink'). When the onset was faster in the lower sink, the main sink initially had a small negative CSD amplitude (current source; for example, **Supplementary Fig. 5** online). We then determined the effect on the onset latency and amplitude of the earliest sink (either main or lower) and the peak of the main current sink of microinjecting either vehicle (artificial cerebrospinal fluid, ACSF) or DHβE (10 μM) directly into or near the STR. Control and drug solutions (~50–60 nl) contained different fluorescent markers, to allow us to identify injection sites later (**Fig. 6a**; see **Supplementary Fig. 6** online for injection types and locations).

Injection of DHβE into the STR delayed the onset and decreased the amplitude of the early current sink that was elicited by characteristic frequency stimuli. DHβE reduced the rising phase of the response to stimuli at 10 dB (**Fig. 6b**) and 20 dB (not shown) above acoustic threshold: onset latencies increased on average by 1.7 ms and 2.0 ms, respectively, and initial (first 5 ms) amplitudes declined by 42% and 51% (see **Supplementary Table 1** online for latency and amplitude measures at each sound intensity tested). These effects differed from those of control injections for responses to near-threshold acoustic stimuli; however, responses to higher intensity stimuli were not affected significantly (**Fig. 6c**,**d**). Application of DHβE to the STR also reduced the peak amplitude of the main current sink (**Fig. 6e**), indicating that reduced thalamocortical input consequently reduces intracortical activity.

Because the STR traverses the posterior portion of the thalamic reticular nucleus (TRN), which provides inhibitory input to MGv, we also targeted this structure (**Supplementary Fig. 6**). Injections of DHβE into the posterior TRN in or near the thalamocortical pathway did not affect the onset latency or initial amplitude of the earliest current sink, or the peak amplitude of the main sink (**Supplementary Fig. 7** online), indicating that blockade of DHβE-sensitive nAChRs in the auditory sector of the TRN or downstream portions of the STR does not influence cortical responses to the acoustic stimuli used here. Similarly, injections of DHβE into other structures adjacent to the STR produced effects that were qualitatively different from those of STR injections (**Supplementary Fig. 6**): injections into the MG proper increased the peak amplitude of the main current sink (to 135.4 ± 15.4% of pre-injection amplitude, $n = 3$; response to 10–60 dB stimuli averaged for each experiment), whereas injections into the lateral portion of the lateral geniculate or hippocampus had no effect (97 ± 1% of pre-injection LFP slope, $n = 3$). Thus, selective blockade of nAChRs in the initial portion of the thalamocortical pathway reduces information transmission to the cortex.

DISCUSSION

These complementary *in vitro* and *in vivo* results show that endogenous ACh activates nAChRs in the initial portion of the auditory thalamocortical pathway to regulate thalamocortical transmission. Nicotinic activation increased axon excitability, decreasing the response threshold in thalamic relay neurons and increasing the probability and synchrony of firing among thalamocortical axons. These effects should reduce the acoustic threshold for cortical neurons and increase the magnitude of sound-evoked cortical responses, consistent with *in vivo* observations. This function of nAChRs is distinct from known

postsynaptic, presynaptic or preterminal mechanisms of nicotinic enhancement[16,17]. The regulation of thalamocortical axon excitability offers a powerful control mechanism, as it occurs after synaptic integration in the thalamus and before the initiation of neurotransmitter release at the terminals.

The effect of nicotine on axon excitability indicates that nAChRs are probably located near nodes of Ranvier along myelinated thalamocortical axons. A decreased response threshold could result from direct depolarization of the axon membrane and/or intracellular signaling following nAChR activation[24–27]. Other possible mechanisms include effects on membrane proteins that control membrane potential[28] or on non-neuronal cells[29]. Notably, changes in excitability persisted for the duration of nicotine application, despite likely desensitization of DHβE-sensitive nAChRs, indicating that stochastic nicotinic activation occurs for the duration of drug perfusion[30], or possibly that there is persistent signaling subsequent to brief nicotinic activation. Desensitization alone is unlikely to increase excitability, for several reasons. First, such a mechanism would imply a previously ongoing—and inhibitory—endogenous nicotinic action that itself did not produce desensitization. Second, DHβE perfusion *in vitro*, which would have blocked any tonic nicotinic action, did not affect success rate. And finally, the effect of DHβE *in vivo* shows that endogenous nicotinic actions are facilitatory, not inhibitory. Future studies will be necessary to elucidate precise mechanisms of enhanced axon excitability.

Our data have several implications for thalamocortical processing. First, if the STR contains the site of initial action potential generation for thalamocortical relay neurons, or if nAChRs are located near the action potential initiation site, then the outcome of thalamic synaptic integration (whether to spike or not) might be regulated by nAChRs. This view is supported by our observations that nicotine enabled previously-subthreshold stimulation to elicit action potentials. Clearly, nAChRs enhance excitability at axon locations that are electrotonically close to somatodendritic inputs[22,23]. In addition, nAChRs enhance the synchrony of discharge, which can increase the efficacy with which cortical neurons are activated, through increased temporal summation[9,10]. Together, the actions of axon-related nAChRs would decrease the acoustic threshold and increase response magnitude for neurons in auditory cortex. Note that our findings do not preclude nicotinic regulation of thalamocortical axons outside the STR, as suggested by recent anatomical studies[18], although the lack of effect of antagonist injections in the downstream STR argue against uniform effects throughout the thalamocortical pathway. Nicotinic regulation might also occur within the cortex, where thalamocortical axons ramify extensively[31,32], although receptors beyond the STR would presumably not regulate the response threshold.

An additional issue raised by our findings concerns the source of endogenous ACh. The nucleus basalis of Meynert and the pedunculopontine and laterodosal tegmental nuclei—brain regions that regulate cognitive function and behavioral state[6,33]—are important sources of cholinergic input to the forebrain[34]. Although the proximity of cholinergic synapses to thalamocortical axons has not been examined, axons that are immunopositive for choline acetyltransferase, the ACh-synthesizing enzyme, are present along the thalamocortical pathway (data not shown). The release of ACh from glia[35,36] remains another potential source of transmitter.

In conclusion, we have identified a new role for nAChRs in regulating cortical information processing by enhancing the excitability of thalamocortical axons. In addition to mediating an endogenous regulatory role, this action might underlie the facilitatory effect of nicotine, the main psychoactive ingredient in tobacco, on sound-evoked cortical potentials[37,38]. Nicotinic enhancement of thalamocortical transmission might improve the selectivity of cortical receptive fields[8,39], and sensory filtering or attentional focus[40,41]. Furthermore, cholinergic regulation of thalamic neurons during different behavioral states[6] could involve nAChRs on thalamocortical axons. These mechanisms might mediate the effects of exogenous nicotine or endogenous ACh on the regulation of sensory-cognitive function.

METHODS

Animals. We used young adult mice (2–3 months old; FVB strain) throughout the experiments. The care and use of animals were approved and reviewed by the Institutional Animal Care and Use Committee of the University of California, Irvine.

Thalamocortical slice preparation. Mice were anesthetized with halothane and decapitated. Brains were quickly removed into cold ACSF containing 125 mM NaCl, 2.5 mM KCl, 25 mM $NaHCO_3$, 1.25 KH_2PO_4, 1.2 mM $MgSO_4$, 2.0 mM $CaCl_2$ and 10 mM dextrose, bubbled with 95% O_2/5% CO_2. Auditory thalamocortical slices ($\sim$450–500 μm) were prepared using a vibroslicer (Leica VT1000) essentially as described for younger animals[19], except that the diagonal cut was made at an angle of 20°, instead of 15°. Slices were placed in a holding chamber containing oxygenated ACSF at room temperature for $>$1 h. To sever thalamocortical axons at the STR, we made a small incision with a blade during slice preparation.

Minimal stimulation experiment. We carried out whole-cell patch recordings as described in the **Supplementary Methods**. We obtained minimally stimulated, presumed monosynaptic, EPSCs by stimulating the STR at 0.l Hz with increasing intensities (1–400 μA; intensity variability depended on electrodes used as well as biological factors) while clamping cells at –70 mV (resting membrane potentials, –71 ± 5 mV) until we observed all-or-none responses. Then, we lowered the stimulation intensity to a point at which no response was observed and then increased it in small increments to examine the range of effective stimulus intensities and probability of success. Typical criteria for minimal responses[4,42–44] were used: (1) all-or-none synaptic events at sub-maximal stimulus intensities; (2) little change in EPSC onset latencies ($<2\times$ s.d.) of the mean of onset latency before drug application; mean latency: 3.71 ± 1.19 ms; mean s.d.: 0.54 ± 0.29 ms); (3) little change in the rise time and half width of EPSCs; (4) little change in onset latency and amplitude with increased stimulus intensity; and (5) little change ($<$0.5 ms) in onset latency to multi-pulse (5–10 pulses at 20 Hz) stimulation. Although the possibility of disynaptic (or multisynaptic) responses exists, the minimal responses could be considered monosynaptic because we observed no apparent doublet (or greater) responses, and no step increase in EPSC amplitude unless stimulus intensity was greatly elevated (presumably recruiting other axons).

Axon spike recordings. Extracellular axon spikes (single units) were recorded in the subcortical white matter using a glass electrode (15–30 μm tip) with or without light suction. When suction was used, we used a water column to maintain sustained negative pressure during recordings. Fibers were visualized using IR-DIC microscopy (40× objective). Signals were amplified and low-pass filtered (6–10 kHz, AI401 headstage, CyberAmp 380), and digitized at 20 kHz. We stimulated the STR as described above. For monopolar stimulation, we used one pole of the parallel bipolar electrode. Axon spikes were identified based on all-or-none responses at threshold, the ability to follow paired-pulses at 100–200 Hz (intensity 10–20% above threshold), and, in some cases, sensitivity to tetrodotoxin ($\sim$1 μM).

For long duration/low intensity stimulation experiments, we first obtained axon spikes with short duration pulses as above to identify them, and then lowered stimulus intensity and prolonged stimulus duration (biphasic stimulus). Axon spikes could be elicited with prolonged duration at intensity below the threshold for 0.2 ms. Onset latency increased as stimulus intensity was lowered. We used stimulus durations of 10–20 ms to accommodate latency delay and variability. The average stimulus intensities for bipolar and monopolar stimulations used for weak intensity/long duration stimulation experiments were 52.5 ± 19.6 μA ($n = 4$, range 24–108 μA) and 18.3 ± 7.4 μA ($n = 5$, range 4.5–40.8 μA), respectively.

***In vitro* data analysis.** Minimally stimulated EPSCs and spontaneous postsynaptic currents were defined as having amplitudes >1.6 times the root mean square of noise[45] and were identified using a template-scaling algorithm (AxoGraph[46]). Response parameters (peak amplitude, onset time, rise time, half width) were measured using AxoGraph.

Axon spikes were visually identified above baseline noise. The onset latency for axon spikes was obtained using AxoGraph at 50% of response peak amplitude.

We calculated the success rates for minimal responses and axon spikes by dividing the number of successful responses by the total number of stimuli (typically 31 for a 5-min bin). We analyzed peak amplitudes and onset latencies for the same data.

To measure relative spread (see **Supplementary Note** online) of stimulus intensity-success rate functions, we fit the data for stimulus intensity and success rate with the following threshold error function (the function of action potential firing probability that follows an integrated Gaussian distribution[47]) using GraphPad Prism (GraphPad Software): $Y = 50\ [1 + \mathrm{erf}\{(X - SI50)\ RS^{-1}\}]$ where Y is success rate, X is normalized stimulus intensity, $SI50$ is the stimulus intensity at which success rate is 50%, RS is the value for relative spread, and $\mathrm{erf}(x)$ is the Gauss error function. We obtained the normalized stimulus intensity (I_s) by normalizing stimulus intensities to the value that gives a 50% success rate.

To assess the effect of nicotine on axon excitability, we examined the change in the threshold function for action potential induction during nicotine perfusion (**Fig. 2e**). We computed normalized stimulus intensities for success rates before nicotine perfusion based on the averaged threshold error function derived in **Figure 1b,** and aligned the success rates on the error function. Success rates for nicotine were plotted directly above the corresponding baseline control (pre-nicotine) data and fitted with the threshold error function equation.

***In vitro* drug application.** We carried out bath perfusion using a single line of tubing with a mixing drip bag before the recording chambers. Drugs were prepared in oxygenated ACSF from stock solutions and perfused. In the submersion recording chamber (~1 ml volume), drug concentration reached about 50, 65 and 75% of the reservoir concentration after 1, 3 and 5 min of perfusion, respectively, as determined by recording the changes in extracellular potential by switching ACSF to a solution containing a one-third concentration of electrolyte.

Local perfusion was accomplished using a single 30 gauge needle (outer diameter 0.3 mm, inner diameter 0.15 mm) connected to a chamber manifold (MPP-4, Warner) and positioned with a micromanipulator. Two syringes (60 ml) containing either oxygenated ACSF or nicotine (1 μM) in the ACSF were connected to the manifold, and either solution was locally perfused by gravity feed. The menisci of the solutions in the syringes were leveled. Flow rate was estimated to be ~0.12 ml min^{-1}. In addition to local perfusion, ACSF was continuously perfused in the bath as described above. During experiments, ACSF was locally perfused for baseline recordings, then switched to nicotine-containing ACSF for 5 min, and then switched back to ACSF for recovery. The perfusion needle in the STR was placed ~0.1 mm from the bipolar stimulus electrode, and at the white matter recording site ~0.1 mm from the recording electrode. At each perfusion site (white matter recording site, STR stimulation site and MGv), the perfusion needle was oriented so that the flow was in the posterior direction away from the thalamocortical pathway (see **Fig. 3c** for the position and orientation of electrodes and the perfusion needle at each of the three sites). See **Supplementary Methods** for control experiment.

***In vivo* electrophysiology.** Mice were anesthetized with urethane (Sigma; 0.7 g kg^{-1} intraperitoneally) and xylazine (Phoenix Pharmaceuticals; 13 mg kg^{-1} intraperitoneally) in saline, placed in a sound-attenuating chamber (IAC) and maintained at 36–37 °C. Anesthesia was supplemented as necessary with 0.13g kg^{-1} urethane and 1.3 mg kg^{-1} xylazine intraperitoneally through a catheter to avoid movement of the mice. A craniotomy was performed and the right auditory cortex was exposed. Acoustic stimuli were presented as described in **Supplementary Methods**. LFPs were recorded with a glass pipette (~1 MΩ at ~1 kHz) or a 16-channel silicon multiprobe (impedance 2–3 MΩ, 100 μm separation; NeuroNexus) and were filtered and amplified (1 Hz to 10 kHz, AI-401 or AI-405 CyberAmp380), digitized (AxoGraph) and stored on a Mac computer.

We determined multiprobe recording sites in the auditory cortex physiologically as follows. The tonotopic characteristic frequency gradient expected for primary auditory cortex was identified using tones in 5-kHz steps at near-threshold intensities (–10 dB to 20 dB sound pressure level (SPL)), and recording in the anterior-posterior (A-P) axis using LFPs on the cortical surface. Reversal of tonotopy, indicating the border with an anterior auditory field, was detected in most cases. Then, we selected a recording site within primary auditory cortex on the basis of the shortest latency and largest amplitude surface LFP to 10–70-dB tones recorded along the dorsal-ventral (D-V) axis. We inserted a multiprobe perpendicular to the pial surface to record LFPs throughout the cortical depth for current source density (CSD) analysis (see below). CSD profiles at recording sites showed fast onset, large current sinks within ~200–400 μm of the pia and smaller, but faster onset sinks ~600–700 μm from the pia (presumably thalamocortical collateral input to the lower layers; see **Supplementary Fig. 5**), indicating that the recordings were from primary auditory cortex[48].

We obtained more precise characteristic frequency and threshold determinations online by analyzing the initial slope of LFPs recorded ~300–400 μm from the pia. LFP initial slopes were measured by finding the maximum slope (0.5–1 ms duration) during the initial rising (or declining) phase (5–10 ms from estimated response onset) of the averaged LFPs. Characteristic frequency was determined in 1-kHz steps as the frequency that elicited the shortest latency LFP at threshold intensity. Threshold intensity at characteristic frequency was determined in 5-dB steps as the lowest intensity to produce LFPs above baseline noise (>3 × s.d. of 100 ms baseline before tone onset) with consistent onset latencies in response to repetitive tone presentation. At threshold, onset latencies averaged 36 ± 4 ms (± s.e.m., $n = 11$).

***In vivo* drug application.** We delivered thalamic microinjections using a 0.5-μl Hamilton syringe fitted with a glass pipette (30–50 μm tip) typically at ~5 nl every 30 s over 5 min. The pipette was backfilled with solutions prepared in ACSF (with 1 or 25 mM $NaHCO_3$) containing either 2% trimethylrhodamine-dextran (10 kD molecular weight, Molecular Probes/Invitrogen) or fluorescin-dextran (10 kD molecular weight, Molecular Probes). DHβE (10 μM) was diluted from 10 mM stock. The solutions were centrifuged at 10,000 rpm for ~3 min and filtered with 0.22-μm nylon filters (Osmonics/Fisher Scientific) before backfilling.

The microinjector was inserted near the STR at stereotaxic coordinates of A-P: 1.5–1.6 mm from Bregma, lateral-medial (L-M): 2.2–2.3 mm, and D-V: 2.8 mm. The coordinates for injection near TRN were 1.0–1.1 mm A-P, 2.5–2.6 mm L-M, and 2.8 mm D-V. The coordinates for injection in MG were 2.2–2.3 mm A-P, 2.4–2.5 mm L-M and 2.8 mm D-V. Baseline LFPs were then recorded by presenting 25 tones per intensity at 0.5 Hz. Different intensities (0–60 dB above threshold) at characteristic frequency were presented sequentially and repeated until stable baseline responses were obtained. We estimated the stability of baseline LFPs online by measuring the initial slope (1–2 ms duration from estimated onsets). After ~5 min of drug injection, recordings resumed immediately and lasted for ~1 h (typically 7–9 repetitions of the intensity sequence at characteristic frequency). The microinjector was then removed. In some experiments, another microinjector was inserted for a second experiment. At the end of experiments, animals were perfused with 4% paraformaldehyde for histochemistry and imaging to localize drug injection sites (see **Supplementary Methods**).

***In vivo* data analysis.** We averaged the LFP traces of 25 tone stimuli recorded in multi-probe channels and carried out CSD analysis on- or off-line using AxoGraph[48,49]. We selected 3–5 main sink CSD traces with stable baseline and consistent sound-evoked responses blind to microinjection solutions and then averaged CSD traces at every probe channel for before (pre) and after (post) microinjection for each experiment ('average CSD trace').

The onset latency of the average CSD trace was defined as the first point of consecutive data points of at least 3 ms duration that were above a threshold amplitude, defined as 2 × s.d. of 7–10 ms baseline before response. The end of the baseline was defined as the onset of the fastest CSD traces found in the lower layers (typically ~600–700 μm below the cortical surface) in response to high intensity tones (60 dB or above) or clicks. We used the same baseline window for onset latency determination for different tone intensities. We calculated the onset latency difference for the early onset sink (**Fig. 6c**) by subtracting pre-injection latency from post-injection latency for each experiment (that is, a positive value means increased latency after injection).

For group average amplitudes of early onset sinks (**Fig. 6b**,**d**), we averaged the amplitudes of the average CSD traces at 5-ms non-overlapping, incremental steps from 15 ms before to 50 ms after the onset of the pre-injection trace (0 ms time point). For initial amplitude changes (**Fig. 6d**), we normalized the group average amplitudes of the first 5 ms (0–5 ms) for post-injection to those for pre-injection. The peak amplitude of the main current sink (**Fig. 6e**) was quantified by averaging the amplitude of a 1 ms duration centered on the peak of the average CSD traces.

Statistical analysis. Statistical comparisons were performed using Microsoft Excel or SPSS. Tests on independent means were Student's *t*-test or factorial ANOVA ($\alpha = 0.05$). Tests on related means were paired *t*-test (two-tail). All mean data are reported ± s.e.m. unless indicated otherwise.

Note: Supplementary information is available on the Nature Neuroscience website.

ACKNOWLEDGMENTS

We thank M. Raastad for technical advice on axon spike recordings, T.J. Carew for comments on an earlier version of manuscript and H.J. Mun and Y. Hu for technical assistance. Supported by US National Institutes of Health grants (DC02967 and DA12929 to R.M., and DC08204 to H.K.).

AUTHOR CONTRIBUTIONS

H.K. conducted the *in vitro* and *in vivo* experiments and data analysis. R.L. contributed to the *in vivo* experiments and data analysis. R.M. supervised the project. H.K. and R.M. co-wrote the manuscript.

COMPETING INTERESTS STATEMENT

The authors declare no competing financial interests.

Published online at http://www.nature.com/natureneuroscience
Reprints and permissions information is available online at http://npg.nature.com/reprintsandpermissions

1. Castro-Alamancos, M.A. & Connors, B.W. Thalamocortical synapses. *Prog. Neurobiol.* **51**, 581–606 (1997).
2. Volgushev, M., Voronin, L.L., Chistiakova, M., Artola, A. & Singer, W. All-or-none excitatory postsynaptic potentials in the rat visual cortex. *Eur. J. Neurosci.* **7**, 1751–1760 (1995).
3. Stratford, K.J., Tarczy-Hornoch, K., Martin, K.A., Bannister, N.J. & Jack, J.J. Excitatory synaptic inputs to spiny stellate cells in cat visual cortex. *Nature* **382**, 258–261 (1996).
4. Gil, Z., Connors, B.W. & Amitai, Y. Efficacy of thalamocortical and intracortical synaptic connections: quanta, innervation and reliability. *Neuron* **23**, 385–397 (1999).
5. McCormick, D.A. Neurotransmitter actions in the thalamus and cerebral cortex and their role in neuromodulation of thalamic activity. *Prog. Neurobiol.* **39**, 337–388 (1992).
6. Steriade, M. Acetylcholine systems and rhythmic activities during the waking-sleep cycle. *Prog. Brain Res.* **145**, 179–196 (2004).
7. Edeline, J.M. The thalamo-cortical auditory receptive fields: regulation by the states of vigilance, learning and the neuromodulatory systems. *Exp. Brain Res.* **153**, 554–572 (2003).
8. Metherate, R. *et al.* Spectral integration in auditory cortex: mechanisms and modulation. *Hear. Res.* **206**, 146–158 (2005).
9. Bruno, R.M. & Sakmann, B. Cortex is driven by weak but synchronously active thalamocortical synapses. *Science* **312**, 1622–1627 (2006).
10. Alonso, J.M., Usrey, W.M. & Reid, R.C. Precisely correlated firing in cells of the lateral geniculate nucleus. *Nature* **383**, 815–819 (1996).
11. McCormick, D.A. & Prince, D.A. Actions of acetylcholine in the guinea-pig and cat medial and lateral geniculate nuclei, *in vitro*. *J. Physiol. (Lond.)* **392**, 147–165 (1987).
12. Curro Dossi, R., Pare, D. & Steriade, M. Short-lasting nicotinic and long-lasting muscarinic depolarizing responses of thalamocortical neurons to stimulation of mesopontine cholinergic nuclei. *J. Neurophysiol.* **65**, 393–406 (1991).
13. Roerig, B., Nelson, D.A. & Katz, L.C. Fast synaptic signaling by nicotinic acetylcholine and serotonin 5–HT3 receptors in developing visual cortex. *J. Neurosci.* **17**, 8353–8362 (1997).
14. Chu, Z.G., Zhou, F.M. & Hablitz, J.J. Nicotinic acetylcholine receptor-mediated synaptic potentials in rat neocortex. *Brain Res.* **887**, 399–405 (2000).
15. Alkondon, M., Pereira, E.F., Eisenberg, H.M. & Albuquerque, E.X. Nicotinic receptor activation in human cerebral cortical interneurons: a mechanism for inhibition and disinhibition of neuronal networks. *J. Neurosci.* **20**, 66–75 (2000).
16. Gil, Z., Connors, B.W. & Amitai, Y. Differential regulation of neocortical synapses by neuromodulators and activity. *Neuron* **19**, 679–686 (1997).
17. Lambe, E.K., Picciotto, M.R. & Aghajanian, G.K. Nicotine induces glutamate release from thalamocortical terminals in prefrontal cortex. *Neuropsychopharmacology* **28**, 216–225 (2003).
18. Ding, Y.S. *et al.* 6-[18F]Fluoro-A-85380, a new PET tracer for the nicotinic acetylcholine receptor: studies in the human brain and *in vivo* demonstration of specific binding in white matter. *Synapse* **53**, 184–189 (2004).
19. Cruikshank, S.J., Rose, H.J. & Metherate, R. Auditory thalamocortical synaptic transmission in vitro. *J. Neurophysiol.* **87**, 361–384 (2002).
20. Rose, H.J. & Metherate, R. Auditory thalamocortical transmission is reliable and temporally precise. *J. Neurophysiol.* **94**, 2019–2030 (2005).
21. Léna, C., Changeux, J.P. & Mulle, C. Evidence for "preterminal" nicotinic receptors on GABAergic axons in the rat interpeduncular nucleus. *J. Neurosci.* **13**, 2680–2688 (1993).
22. Alle, H. & Geiger, J.R. Combined analog and action potential coding in hippocampal mossy fibers. *Science* **311**, 1290–1293 (2006).
23. Shu, Y., Hasenstaub, A., Duque, A., Yu, Y. & McCormick, D.A. Modulation of intracortical synaptic potentials by presynaptic somatic membrane potential. *Nature* **441**, 761–765 (2006).
24. Armett, C.J. & Ritchie, J.M. The action of acetylcholine and some related substances on conduction in mammalian non-myelinated nerve fibres. *J. Physiol. (Lond.)* **155**, 372–384 (1961).
25. Brown, D.A., Docherty, R.J. & Halliwell, J.V. The action of cholinomimetic substances on impulse conduction in the habenulointerpeduncular pathway of the rat *in vitro*. *J. Physiol. (Lond.)* **353**, 101–109 (1984).
26. Lang, P.M. *et al.* Characterization of neuronal nicotinic acetylcholine receptors in the membrane of unmyelinated human C-fiber axons by *in vitro* studies. *J. Neurophysiol.* **90**, 3295–3303 (2003).
27. Zhang, C.L., Verbny, Y., Malek, S.A., Stys, P.K. & Chiu, S.Y. Nicotinic acetylcholine receptors in mouse and rat optic nerves. *J. Neurophysiol.* **91**, 1025–1035 (2004).
28. Waxman, S.G. & Ritchie, J.M. Molecular dissection of the myelinated axon. *Ann. Neurol.* **33**, 121–136 (1993).
29. Rawlins, F.A. & Villegas, J. Autoradiographic localization of acetylcholine receptors in the Schwann cell membrane of the squid nerve fiber. *J. Cell Biol.* **77**, 371–376 (1978).
30. Pidoplichko, V.I., DeBiasi, M., Williams, J.T. & Dani, J.A. Nicotine activates and desensitizes midbrain dopamine neurons. *Nature* **390**, 401–404 (1997).
31. Hashikawa, T., Molinari, M., Rausell, E. & Jones, E.G. Patchy and laminar terminations of medial geniculate axons in monkey auditory cortex. *J. Comp. Neurol.* **362**, 195–208 (1995).
32. Huang, C.L. & Winer, J.A. Auditory thalamocortical projections in the cat: laminar and areal patterns of input. *J. Comp. Neurol.* **427**, 302–331 (2000).
33. Sarter, M. & Bruno, J.P. Cortical cholinergic inputs mediating arousal, attentional processing and dreaming: differential afferent regulation of the basal forebrain by telencephalic and brainstem afferents. *Neuroscience* **95**, 933–952 (2000).
34. Mesulam, M.M., Mufson, E.J., Wainer, B.H. & Levey, A.I. Central cholinergic pathways in the rat: an overview based on an alternative nomenclature (Ch1-Ch6). *Neuroscience* **10**, 1185–1201 (1983).
35. Lan, C.T., Shieh, J.Y., Wen, C.Y., Tan, C.K. & Ling, E.A. Ultrastructural localization of acetylcholinesterase and choline acetyltransferase in oligodendrocytes, glioblasts and vascular endothelial cells in the external cuneate nucleus of the gerbil. *Anat. Embryol. (Berl.)* **194**, 177–185 (1996).
36. Wessler, I. *et al.* Mammalian glial cells in culture synthesize acetylcholine. *Naunyn Schmiedebergs Arch. Pharmacol.* **356**, 694–697 (1997).
37. Harkrider, A.W. & Champlin, C.A. Acute effect of nicotine on non-smokers: II. MLRs and 40-Hz responses. *Hear. Res.* **160**, 89–98 (2001).
38. Domino, E.F. Effects of tobacco smoking on electroencephalographic, auditory evoked and event related potentials. *Brain Cogn.* **53**, 66–74 (2003).
39. Liang, K. *et al.* Neonatal nicotine exposure impairs nicotinic enhancement of central auditory processing and auditory learning in adult rats. *Eur. J. Neurosci.* **24**, 857–866 (2006).
40. Friedman, J., Horvath, T. & Meares, R. Tobacco smoking and a 'stimulus barrier'. *Nature* **248**, 455–456 (1974).
41. Knott, V.J. Tobacco effects on cortical evoked potentials to distracting stimuli. *Neuropsychobiology* **13**, 74–80 (1985).
42. Raastad, M., Storm, J.F. & Andersen, P. Putative single quantum and single fibre excitatory postsynaptic currents show similar amplitude range and variability in rat hippocampal slices. *Eur. J. Neurosci.* **4**, 113–117 (1992).
43. Allen, C. & Stevens, C.F. An evaluation of causes for unreliability of synaptic transmission. *Proc. Natl. Acad. Sci. USA* **91**, 10380–10383 (1994).
44. Dobrunz, L.E. & Stevens, C.F. Heterogeneity of release probability, facilitation, and depletion at central synapses. *Neuron* **18**, 995–1008 (1997).
45. Markram, H., Lubke, J., Frotscher, M., Roth, A. & Sakmann, B. Physiology and anatomy of synaptic connections between thick tufted pyramidal neurones in the developing rat neocortex. *J. Physiol. (Lond.)* **500**, 409–440 (1997).
46. Clements, J.D. & Bekkers, J.M. Detection of spontaneous synaptic events with an optimally scaled template. *Biophys. J.* **73**, 220–229 (1997).
47. White, J.A., Rubinstein, J.T. & Kay, A.R. Channel noise in neurons. *Trends Neurosci.* **23**, 131–137 (2000).
48. Müller-Preuss, P. & Mitzdorf, U. Functional anatomy of the inferior colliculus and the auditory cortex: current source density analyses of click-evoked potentials. *Hear. Res.* **16**, 133–142 (1984).
49. Kaur, S., Rose, H.J., Lazar, R., Liang, K. & Metherate, R. Spectral integration in primary auditory cortex: laminar processing of afferent input, *in vivo* and *in vitro*. *Neuroscience* **134**, 1033–1045 (2005).